

Finite-mass effects on inclusive B -meson hadroproduction

Bernd A. Kniehl* and Gustav Kramer†

II. Institut für Theoretische Physik, Universität Hamburg, Luruper Chaussee 149, 22761 Hamburg, Germany

Ingo Schienbein‡

Laboratoire de Physique Subatomique et de Cosmologie, Université Joseph Fourier Grenoble 1, CNRS/IN2P3, Institut National Polytechnique de Grenoble, 53 avenue des Martyrs, 38026 Grenoble, France

Hubert Spiesberger§

Institut für Physik, Johannes-Gutenberg-Universität, Staudinger Weg 7, 55099 Mainz, Germany

(Received 30 May 2007; published 11 January 2008)

We calculate the transverse-momentum (p_T) distribution for the inclusive hadroproduction of B mesons at intermediate values of p_T at next-to-leading order (NLO) in a dedicated finite-mass scheme using realistic nonperturbative fragmentation functions that are obtained through a global fit to e^+e^- data from CERN LEP1 and SLAC SLC exploiting their universality and scaling violations. We find that finite-mass effects moderately enhance the cross section, by about 20% at $p_T = 2m_b$, and rapidly fade out with increasing value of p_T , so that the zero-mass prediction is reached. We also perform comparisons with recent $p\bar{p}$ data taken by the CDF Collaboration in run II at the Fermilab Tevatron and comment on the usefulness of the fixed-flavor-number scheme.

DOI: [10.1103/PhysRevD.77.014011](https://doi.org/10.1103/PhysRevD.77.014011)

PACS numbers: 12.38.Bx, 13.85.Ni, 13.87.Fh, 14.40.Nd

I. INTRODUCTION

Recently there has been much interest in the study of B -meson production in $p\bar{p}$ collisions at hadron colliders, both experimentally and theoretically. The CDF Collaboration measured differential cross sections $d\sigma/dp_T$ for the inclusive production of B mesons (and their antiparticles) in $p\bar{p}$ collisions at the Fermilab Tevatron as a function of the transverse momentum p_T in the central rapidity (y) region [1–4]. The data reported in Ref. [1] were collected in the run period from 1992 to 1995 (runs IA and I) at a center-of-mass (c.m.) energy of $\sqrt{s} = 1.8$ TeV and were obtained using fully reconstructed B^\pm mesons decaying into the exclusive final state $J/\psi K^\pm$. The data presented in Ref. [2] come from measurements in run II with $\sqrt{s} = 1.96$ TeV where the inclusive differential production cross section of J/ψ mesons was used and the fraction of events from the decay of long-lived b hadrons was separated by analyzing the lifetime distribution. These b hadrons include B^+ , B^- , B^0 , and \bar{B}^0 mesons. The data in Ref. [3] were also taken at $\sqrt{s} = 1.96$ TeV in run II. In this case, the inclusive cross section for the production of B^\pm mesons was obtained, as in Ref. [1], by reconstructing $B^\pm \rightarrow J/\psi K^\pm$ decays. Very recently, CDF presented preliminary data from run II based on events with $B^- \rightarrow D^0 \mu^- \bar{\nu}_\mu$ followed by $D^0 \rightarrow K^- \pi^+$ and $B^- \rightarrow D^{*+} \mu^- \bar{\nu}_\mu$ followed by $D^{*+} \rightarrow D^0 \pi^+$ and $D^0 \rightarrow K^- \pi^+$

collected with the lepton-plus-displaced-track trigger [4]. These data explore the range $25 \text{ GeV} < p_T < 40 \text{ GeV}$ for the first time. Although the measurement of B mesons is experimentally well defined, theoretical predictions did not agree with the data in the past.

In order to calculate the B -meson production cross section, the nonperturbative fragmentation function (FF) for the transition $b \rightarrow B$ must be known beforehand. The QCD-improved parton model implemented in the modified minimal-subtraction ($\overline{\text{MS}}$) renormalization and factorization scheme then provides a rigorous theoretical framework for a coherent global data analysis.

In this framework, two distinct approaches for next-to-leading-order (NLO) calculations in perturbative QCD have been used for comparisons with experimental data. In the so-called massless scheme or zero-mass variable-flavor-number scheme (ZM-VFNS) [5–7], which is the conventional parton model approach, the zero-mass-parton approximation is applied also to the b quark, although its mass m is certainly much larger than the asymptotic scale parameter Λ_{QCD} . In this approach, the b quark is also treated as an incoming parton originating from the (anti)proton, leading to additional contributions besides those from u , d , s , and c quarks and the gluon (g). Although this approach can be used as soon as the factorization scales associated with the initial- and final-state singularities are above the starting scale of the parton distribution functions (PDFs) and the FFs, the predictions are reliable only in the region of large p_T values, with $p_T \gg m$, where terms of the order of m^2/p_T^2 can safely be neglected. A NLO calculation in this scheme automatically resums leading and next-to-leading logarithms (NLL), i.e. terms of the

*bernd.kniehl@desy.de

†gustav.kramer@desy.de

‡schien@lpsc.in2p3.fr

§hspiesb@thep.physik.uni-mainz.de

form $[\alpha_s \ln(p_T^2/m^2)]^n$ and $\alpha_s[\alpha_s \ln(p_T^2/m^2)]^n$ with $n = 1, 2, 3, \dots$, where α_s is the strong-coupling constant. At the same time, all nonlogarithmic terms through $\mathcal{O}(\alpha_s)$ relative to the Born approximation are retained for $m = 0$ [8].

The other calculational scheme is the so-called massive scheme or fixed-flavor-number scheme (FFNS) [9], in which the number of active flavors in the initial state is limited to $n_f = 4$, and the b quark appears only in the final state. In this case, the b quark is always treated as a heavy particle, not as a parton. The actual mass parameter m is explicitly taken into account along with p_T . In this scheme, m acts as a cutoff for the initial- and final-state collinear singularities and sets the scale for the perturbative calculations. A factorization of these would-be initial- and final-state collinear singularities is not necessary, neither is the introduction of a FF for the transition $b \rightarrow B$. However, at NLO, terms proportional to $\alpha_s \ln(p_T^2/m^2)$ arise from collinear gluon emissions by b quarks or from branchings of gluons into collinear $b\bar{b}$ pairs. These terms are of order $\mathcal{O}(1)$ for large values of p_T , and with the choice $\mu_R = \mathcal{O}(p_T)$ for the renormalization scale they spoil the convergence of the perturbation series. The FFNS with $n_f = 4$ should thus be limited to a rather small range of p_T , from $p_T = 0$ to $p_T \gtrsim m$. The advantage of this scheme is that the m^2/p_T^2 power terms are fully taken into account.

The ZM-VFNS and FFNS are valid in complementary regions of p_T , and it is desirable to combine them in a unified approach that incorporates the virtues of both schemes, i.e. to resum the large logarithms, retain the full finite- m effects, and preserve the universality of the FFs. This is necessary for a reliable and meaningful interpretation of the published CDF data [1–3], which mostly lie in the transition region of the two schemes. An earlier approach to implement such an interpolation is the so-called fixed-order-next-to-leading-logarithm (FONLL) scheme, in which the conventional cross section in the FFNS is linearly combined with a suitably modified cross section in the ZM-VFNS with perturbative FFs, using a p_T -dependent weight function [10,11]. Then the FONLL cross section is convoluted with a nonperturbative FF for the $b \rightarrow B$ transition. These FFs are adjusted to e^+e^- data, using the same approach, and good agreement with the CDF data was obtained.

In this work, we wish to present the results of an approach that is much closer in spirit to the ZM-VFNS, but keeps all m^2/p_T^2 power terms in the hard-scattering cross sections. This scheme is called general-mass variable-flavor-number scheme (GM-VFNS) and has recently been worked out for the photoproduction [12,13] and hadroproduction [14–16] of charmed hadrons. In this approach, one starts from the region $p_T \gg m$ and absorbs the large logarithms $\ln(\mu_F^2/m^2)$, where μ_F is the factorization scale of the initial or final state, into the b -quark PDF of the incoming hadrons and the FF for the $b \rightarrow B$ transition.

After factorizing the $\ln m^2$ terms, the cross section is infra-red safe in the limit $m \rightarrow 0$, and $n_f = 5$ is taken in the strong-coupling constant and the Dokshitzer-Gribov-Lipatov-Altarelli-Parisi (DGLAP) evolution equations. The remaining m -dependent contributions, i.e. the m^2/p_T^2 power terms, are retained in the hard-scattering cross sections. These terms are very important in the region of intermediate p_T values, $p_T \gtrsim m$, and are expected to improve the theoretical predictions as compared to the ZM-VFNS. The large logarithms are absorbed into the PDFs and FFs by subtraction of the collinearly (mass) singular terms at the initial- and final-state factorization scales, respectively.

It is well known that the subtraction of just the collinearly, i.e. mass singular terms, does not define a unique factorization prescription. Also finite terms must be specified. In the conventional ZM-VFNS calculation, one puts $m = 0$ from the beginning, and the collinearly divergent terms are defined with the help of dimensional regularization. This fixes the finite terms in a specific way, and their form is inherent to the chosen regularization procedure. If one starts with $m \neq 0$ and performs the limit $m \rightarrow 0$ afterwards, the finite terms are different. These terms have to be removed by subtraction together with the $\ln m^2$ terms in such a way that, in the limit $p_T \rightarrow \infty$, the known massless $\overline{\text{MS}}$ expressions are recovered. This matching procedure is needed, since we use PDFs and FFs defined in the ZM-VFNS. A subtraction scheme defined in this way is the correct extension of the conventional ZM-VFNS to include b -quark (or similarly c -quark) mass effects in a consistent way. We actually include the c -quark contribution in the massless approximation, i.e. we treat the c quark as one of the light partons.

The results of our earlier work on charmed-hadron inclusive production by $p\bar{p}$ scattering at NLO in the GM-VFNS [14–16] directly carry over to b hadrons. Then, the b quark is the heavy one, with mass m , while the c quark belongs to the group of light quarks, collectively denoted by $q = u, d, s, c$ in the following, whose mass is put to zero. Furthermore, we need PDFs and FFs implemented with $n_f = 5$ in the $\overline{\text{MS}}$ factorization scheme. Nonperturbative FFs for the transitions $a \rightarrow B^\pm$, where $a = g, q, \bar{q}, b, \bar{b}$, were extracted at leading order (LO) and NLO already several years ago [5] using data for the scaled-energy (x) distribution $d\sigma/dx$ of $e^+e^- \rightarrow B + X$ at $\sqrt{S} = 91.2$ GeV measured by the OPAL Collaboration at CERN LEP1 [17].

We note that our implementation of the GM-VFNS is similar to the Aivazis-Collins-Olness-Tung (ACOT) [18] scheme formulated for the initial state of fully inclusive deep-inelastic scattering. The extension of this scheme to the inclusive production of heavy partons was considered in Ref. [19], where the resummation of the final-state collinear logarithms was only performed to LO and parton-to-hadron FFs were not included. A discussion of the differ-

ences between our approach and the one in Ref. [19] concerning the collinear subtraction terms can be found in Ref. [15].

This paper is organized as follows. In Sec. II, we introduce new NLO sets of B -meson FFs. In Sec. III, we numerically analyze the GM-VFNS predictions with regard to the impact of the m -dependent terms and the relative importance of the various partonic initial states. In Sec. IV, we compare the predictions of the GM-VFNS, and also those of the ZM-VFNS and FFNS, with CDF data from run II [2–4]. Our conclusions are contained in Sec. V.

II. NONPERTURBATIVE B -MESON FRAGMENTATION FUNCTION

As input for the calculation of inclusive B -meson production cross sections one needs a realistic nonperturbative FF describing the transition of the b (\bar{b}) quark into a B meson. Such a FF can be obtained only from experiment. In Ref. [5], LEP1 data for the distribution in the scaled B -meson energy, $x = 2E_B/\sqrt{S}$, from OPAL [17] were fitted at LO and NLO in the ZM-VFNS using three different ansätze for the $b \rightarrow B$ FF at the starting scale $\mu_F = \mu_0$ of the DGLAP evolution, including the ansatz by Peterson *et al.* [20],

$$D(x, \mu_0^2) = N \frac{x(1-x)^2}{[(1-x)^2 + \epsilon x]^2}, \quad (1)$$

and the simple power ansatz [21],

$$D(x, \mu_0^2) = N x^\alpha (1-x)^\beta. \quad (2)$$

The best fit was obtained for the Peterson ansatz. In Ref. [5], the starting scale was taken to be $\mu_0 = 2m$, with $m = 5.0$ GeV. The $a \rightarrow B$ FFs for $a = g, q, \bar{q}$ were assumed to be zero at $\mu_F = \mu_0$ and generated through the DGLAP evolution to larger values of μ_F .

In the meantime, new and more precise measurements of the cross section of inclusive B -meson production in e^+e^- annihilation on the Z -boson resonance have been published by the ALEPH [22], OPAL [23], and SLD [24] collaborations, which motivates us to update the analysis of Ref. [5]. This also gives us the opportunity to adjust some of the choices made in Ref. [5], to conform with the conventions underlying modern PDF sets. In fact, for our numerical analysis, we use the NLO proton PDF set CTEQ6.1M, based on the $\overline{\text{MS}}$ prescription, by the Coordinated Theoretical-Experimental Project on QCD (CTEQ) [25]. In this set, the b -quark PDF has its starting scale at $\mu_0 = m$ with $m = 4.5$ GeV. The mass values used in PDFs and FFs have, of course, to be chosen consistently in order to avoid the appearance of terms proportional to $\ln(\mu_0^2/m^2)$ in the NLO corrections. While a shift in the starting scale from $\mu_0 = 2m$ with $m = 5.0$ GeV to $\mu_0 = m$ with $m = 4.5$ GeV changes the b -quark FFs only marginally at μ_F values relevant for the e^+e^- annihilation

cross sections to be used in the fit, it does have a significant effect on the $g \rightarrow B$ FF, which greatly affects the cross section predictions for the Tevatron. The size of the analogous effect for D^{*+} FFs is investigated in Fig. 1 of Ref. [26], which uses $\mu_0 = m_c$, through comparison with Ref. [27], which uses $\mu_0 = 2m_c$. We thus perform a combined fit to these three data sets [22–24] using $\mu_0 = m$ with $m = 4.5$ GeV as in Ref. [25]. Furthermore, we adopt from Ref. [25] the NLO value $\Lambda_{\overline{\text{MS}}}^{(5)} = 227$ MeV appropriate for $n_f = 5$, which corresponds to $\alpha_s^{(5)}(m_Z) = 0.1181$. As in Ref. [5], we chose the renormalization and factorization scales to be $\mu_R = \mu_F = \sqrt{S}$. We use the ansätze of Eqs. (1) and (2) for the $b \rightarrow B$ FF at $\mu_F = \mu_0$, while the $g, q \rightarrow B$ FFs are taken to vanish at $\mu_F = \mu_0$ and are generated through the DGLAP evolution. In order to obtain acceptable fits, we have to omit some of the data points in the small- x region. Specifically, we only include the ALEPH data with $x \geq 0.25$, the OPAL data with $x \geq 0.325$, and the SLD data with $x \geq 0.28$. At the other end of the x range, we include all data points up to $x = 1$. Altogether we use 18, 15, and 18 data points of the ALEPH, OPAL, and SLD sets, respectively. Since we only include in the fit data from the Z -boson resonance, finite- m effects, being of relative order $m_b^2/m_Z^2 = 0.2\%$, are greatly suppressed, so that we are comfortably within the asymptotic regime where the GM-VFNS is equivalent to the ZM-VFNS.

The values of the parameters in Eqs. (1) and (2) obtained through the fits based on the Peterson and power ansätze are listed in Table I together with the respective values of χ^2 per degree of freedom, $\chi^2/\text{d.o.f}$. The corresponding $d\sigma/dx$ distributions are compared with the ALEPH [22], OPAL [23], and SLD [24] data in Fig. 1. These three data sets mostly overlap and can hardly be distinguished in the figure. We observe from Table I and Fig. 1 that the power ansatz yields an excellent overall fit to the selected data points. There are deviations at $x \leq 0.3$, which are due to the exclusion of data points from the fit. The $\chi^2/\text{d.o.f}$ value for the combined fit is 1.495. The individual $\chi^2/\text{d.o.f}$ values of the ALEPH, OPAL, and SLD data sets are 0.861, 2.350, and 1.410, respectively. On the other hand, the Peterson ansatz leads to an intolerable description of the data, yielding $\chi^2/\text{d.o.f} = 21.37$ for the combined fit and similar values for the individual data sets. This ansatz has only two free parameters, N and ϵ , and is just not flexible enough to account for the very precise experimental data.

TABLE I. Fit parameters of the b -quark FFs in Eqs. (1) and (2) at the starting scale $\mu_0 = m = 4.5$ GeV and values of $\chi_{\text{d.o.f}}^2$ achieved. All other FFs are taken to be zero at $\mu_0 = m$.

N	α	β	ϵ	$\chi^2/\text{d.o.f}$
0.066 34	—	—	0.008 548	21.37
4684.1	16.87	2.628	—	1.495

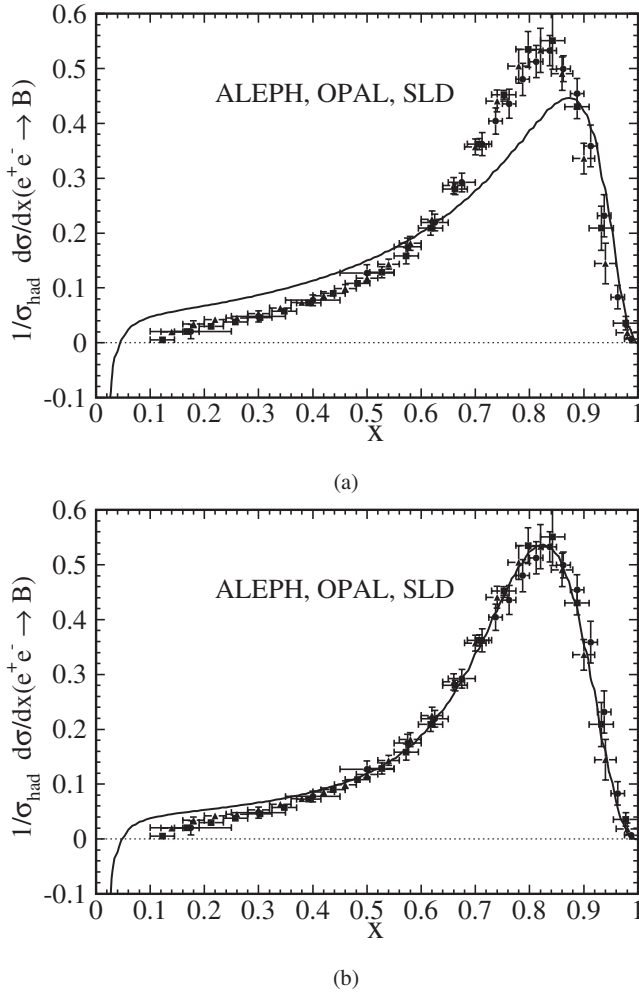


FIG. 1. Comparisons of the ALEPH [22] (circles), OPAL [23] (squares), and SLD [24] (triangles) data with the NLO fits using (a) the Peterson ansatz (1) and (b) the power ansatz (2). The initial factorization scale for all partons is $\mu_0 = m = 4.5$ GeV. The different symbols can be better distinguished in the electronic edition, where the figures can be enlarged.

Besides the $b \rightarrow B$ FF itself, also its first two moments are of phenomenological interest and subject to experimental determination. They correspond to the $b \rightarrow B$ branching fraction,

$$B(\mu_F) = \int_{x_{\text{cut}}}^1 dx D(x, \mu_F^2), \quad (3)$$

and the average energy fraction that the B meson receives from the b quark,

$$\langle x \rangle(\mu_F) = \frac{1}{B(\mu_F)} \int_{x_{\text{cut}}}^1 dx x D(x, \mu_F^2), \quad (4)$$

where the cut $x_{\text{cut}} = 0.15$ excludes the x range where our formalism is not valid. We observe from Table II that the Peterson and power ansatz lead to rather similar results for $B(\mu_F)$ and $\langle x \rangle(\mu_F)$, the ones for the power

TABLE II. Branching fractions $B(\mu_F)$ and average energy fractions $\langle x \rangle(\mu_F)$ evaluated at factorization scales $\mu_F = 4.5, 9.0,$ and 91.2 GeV using the $b \rightarrow B$ FFs based on the Peterson and power ansatz.

μ_F (in GeV)	Peterson		power	
	$B(\mu_F)$	$\langle x \rangle(\mu_F)$	$B(\mu_F)$	$\langle x \rangle(\mu_F)$
4.5	0.3994	0.8098	0.4007	0.8312
9.0	0.3935	0.7542	0.3955	0.7730
91.2	0.3767	0.6403	0.3803	0.6537

ansatz being slightly larger. While $B(\mu_F)$ is practically independent of μ_F , $\langle x \rangle(\mu_F)$ is shifted towards smaller values through the evolution in μ_F . It is interesting to compare the results for $\langle x \rangle(91.2 \text{ GeV})$ in Table II with the values quoted by ALEPH, OPAL, and SLD, which read 0.7361 ± 0.0061 (stat) ± 0.0056 (syst) [22], 0.7193 ± 0.0016 (stat) $^{+0.0036}_{-0.0031}$ (syst) [23], and 0.709 ± 0.003 (stat) ± 0.003 (syst) ± 0.002 (model) [24], respectively. We observe that the experimental results lie systematically above ours. However, one must keep in mind that the experimental results refer to the first moment of the measured cross section distribution $d\sigma/dx$, which naturally includes all orders and also contributions from gluon and light-quark fragmentation, while ours are evaluated from the $b \rightarrow B$ FF at NLO in the $\overline{\text{MS}}$ scheme via Eq. (4). Of course, the $b \rightarrow B$ FF and its moments depend on scheme, order, and implementation issues such as the functional form of the ansatz at the starting scale μ_0 and the value of μ_0 itself, and thus do not represent physical observables by themselves. Nevertheless, comparisons of the quantities $B(\mu_F)$ and $\langle x \rangle(\mu_F)$ defined in Eqs. (3) and (4), respectively, with their experimental counterparts are useful to check the dominance of $b \rightarrow B$ fragmentation and are routinely performed in the literature (see, e.g., Ref. [5]).

III. THEORETICAL PREDICTIONS FOR $p\bar{p} \rightarrow B + X$

We are now in a position to perform a numerical analysis. We consider the inclusive cross section of $p\bar{p} \rightarrow B + X$, where B stands for the average of the B^+ and B^- mesons, at $\sqrt{S} = 1.96$ TeV as in run II at the Tevatron. We concentrate on the p_T distribution integrated over $|y| < 1$ corresponding to the central region of the CDF detector. We use the CTEQ6.1M proton PDFs [25] and the B -meson FFs based on the power ansatz presented in Sec. II, both implemented at NLO with $\Lambda_{\overline{\text{MS}}}^{(5)} = 227$ MeV and $m = 4.5$ GeV. For simplicity, we use a common factorization scale for the initial and final states. We set the renormalization and factorization scales to $\mu_R = \xi_R m_T$ and $\mu_F = \xi_F m_T$, where $m_T = \sqrt{p_T^2 + m^2}$ is the transverse mass of the b quark and ξ_R and ξ_F are introduced to estimate the theoretical uncertainty. Unless otherwise stated, we use the

default values $\xi_R = \xi_F = 1$. With our default choices $\mu_0 = m$ and $\mu_F = m_T$, we have $\mu_F \rightarrow \mu_0$ as $p_T \rightarrow 0$. In this limit, the FFs and b -quark PDF should fade out and quench the cross section, leading to a turnover of the p_T distribution. However, the precise location of the maximum and other details of the line shape are also subject to other implementation issues of the GM-VFNS. We shall return to this topic in Sec. IV.

The calculation of the cross section $d^2\sigma/(dp_T dy)$ of B -meson hadroproduction at NLO in the GM-VFNS proceeds analogously to the case of D mesons outlined in Ref. [14]. Now, m denotes the mass of the b quark, and the c quark belongs to the group of light quarks q , whose masses are put to zero. The NLO cross section consists of three classes of contributions.

- (1) Class (i) contains all the partonic subprocesses with a $b, \bar{b} \rightarrow B$ transition in the final state that have only light partons (g, q, \bar{q}) in the initial state, the possible pairings being $gg, gq, g\bar{q}$, and $q\bar{q}$. A Feynman diagram representing this class is shown in Fig. 2(a).
- (2) Class (ii) contains all the partonic subprocesses with a $b, \bar{b} \rightarrow B$ transition in the final state that also have b or \bar{b} quarks in the initial state, the possible pairings being $gb, g\bar{b}, qb, q\bar{b}, \bar{q}b, \bar{q}\bar{b}$, and $b\bar{b}$ [see Fig. 2(b)].
- (3) Class (iii) contains all the partonic subprocesses with a $g, q, \bar{q} \rightarrow B$ transition in the final state [see Fig. 2(c)].

In the FFNS, only the contribution of class (i) is included, but the full m dependence is retained [9]. On the other hand, in the ZM-VFNS, the contributions of all three classes are taken into account, but they are evaluated for $m = 0$ [28]. In the GM-VFNS, the class-(i) contribution of the FFNS is matched to the $\overline{\text{MS}}$ scheme, through appro-

prate subtractions of would-be collinear singularities, and is then combined with the class-(ii) and class-(iii) contributions of the ZM-VFNS; thus, only the hard-scattering cross sections of class (i) carry explicit m dependence. Specifically, the subtractions affect initial states involving $g \rightarrow b\bar{b}$ splittings and final states involving $g \rightarrow b\bar{b}$, $b \rightarrow gb$, and $\bar{b} \rightarrow g\bar{b}$ splittings, and they introduce logarithmic dependences on the initial- and final-state factorization scales in the hard-scattering cross sections of class (i), which are compensated through NLO by the respective factorization scale dependences of the b -quark PDF and the $b \rightarrow B$ FF, respectively. The explicit form of the subtractions may be found in Ref. [15]. A certain part of the class-(ii) and class-(iii) contributions is due to Feynman diagrams with internal b -quark lines; another one is due to diagrams with external b -quark lines and contains m -dependent logarithms, which are resummed. In the FFNS, the m dependence of these contributions would only enter beyond NLO, which is reflected in the ZM-VFNS by the generic suppression of the b -quark PDF relative to the gluon and q -quark ones and of the gluon and q -quark FFs relative to the b -quark one. This entitles us to omit this m dependence by calculating the contributions of classes (ii) and (iii) in the ZM-VFNS. It turns out that q -quark fragmentation contributes negligibly. However, the gluon fragmentation contribution reaches approximately 50% at small values of p_T , and its relative contribution decreases only rather mildly towards larger values of p_T .

We first investigate the effect of the finite- m terms in the hard-scattering cross sections and thus concentrate on the contribution of class (i) for the time being. This effect can already be studied at LO, where the partonic subprocesses read $g + g \rightarrow b + \bar{b}$ and $q + \bar{q} \rightarrow b + \bar{b}$. To this end, we

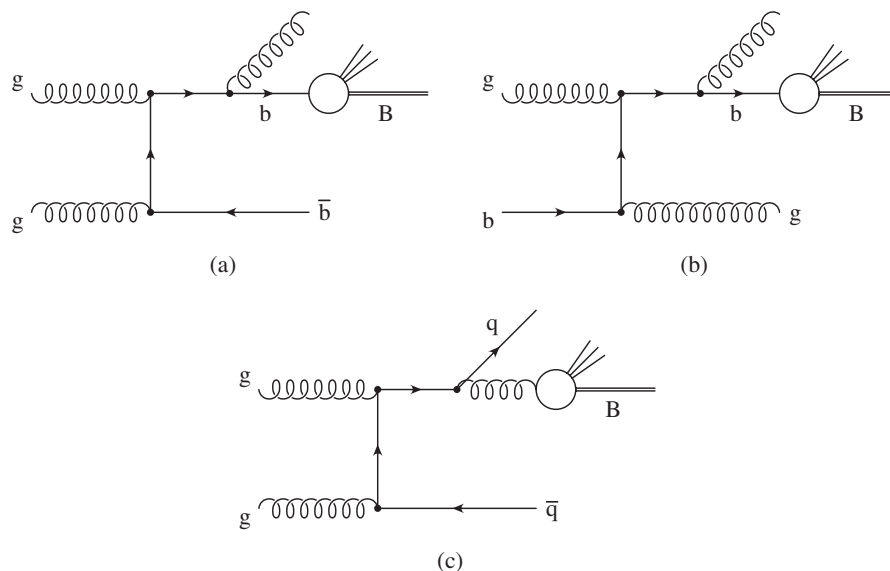


FIG. 2. Examples of Feynman diagrams leading to contributions of (a) class (i), (b) class (ii), and (c) class (iii).

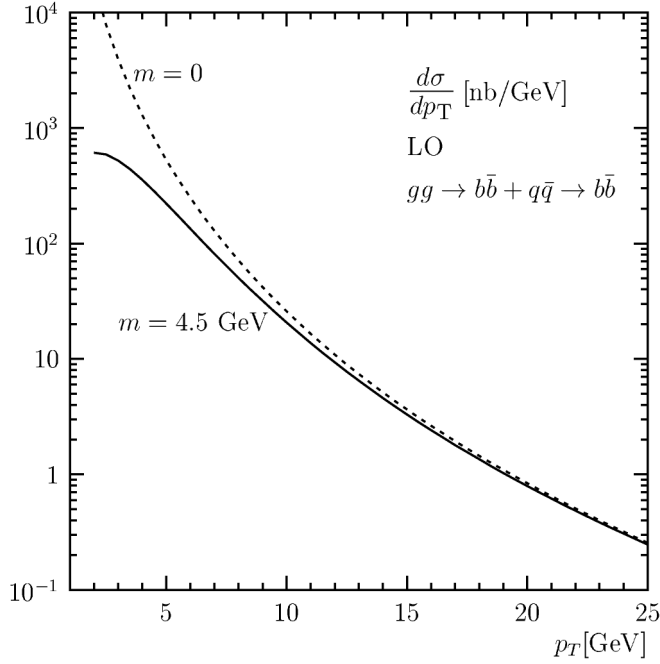


FIG. 3. Transverse-momentum distribution $d\sigma/dp_T$ of $p\bar{p} \rightarrow B + X$ at c.m. energy $\sqrt{S} = 1.96$ TeV integrated over the rapidity range $|y| < 1$. The contributions of class (i) evaluated at LO in the ZM-VFNS (dashed line) and the GM-VFNS (solid line), but with the NLO versions of α_s , the PDFs, and the FFs, are compared.

simply switch off the NLO terms in the hard-scattering cross sections while keeping α_s , the PDFs, and the FFs at NLO, although, strictly speaking, this does not represent a genuine LO analysis. The results are shown in Fig. 3, where the dashed and solid lines refer to the results for zero and finite values of m , respectively. We observe that these results rapidly approach each other with increasing value of p_T . At $p_T = 7.5$ GeV, the finite- m result is 33% smaller than the $m = 0$ one, a relative difference of the order of m^2/p_T^2 , as expected.

We now turn to NLO by switching on the QCD corrections to the hard-scattering cross sections of class (i). The results for $m = 0$ and finite m are shown in Fig. 4 as the upper and lower solid lines, respectively. They constitute parts of the final ZM-VFNS and GM-VFNS results. In both cases, the contributions of classes (ii) and (iii) for $m = 0$ still must be added to obtain the full predictions to be compared with experimental data. The class-(i) contributions in the ZM-VFNS and GM-VFNS schemes are, therefore, entitled to be negative and they indeed are, for $p_T \lesssim 76$ GeV and $p_T \lesssim 10$ GeV, respectively, as may be seen from Fig. 4. Comparing the ZM-VFNS and GM-VFNS results, we notice that the finite- m effects are significant for $p_T \lesssim 10$ GeV and even cause a sign change for $10 \text{ GeV} \lesssim p_T \lesssim 76$ GeV. However, as will become apparent below, the contributions of class (i) are overwhelmed by those of classes (ii) and (iii), so that the

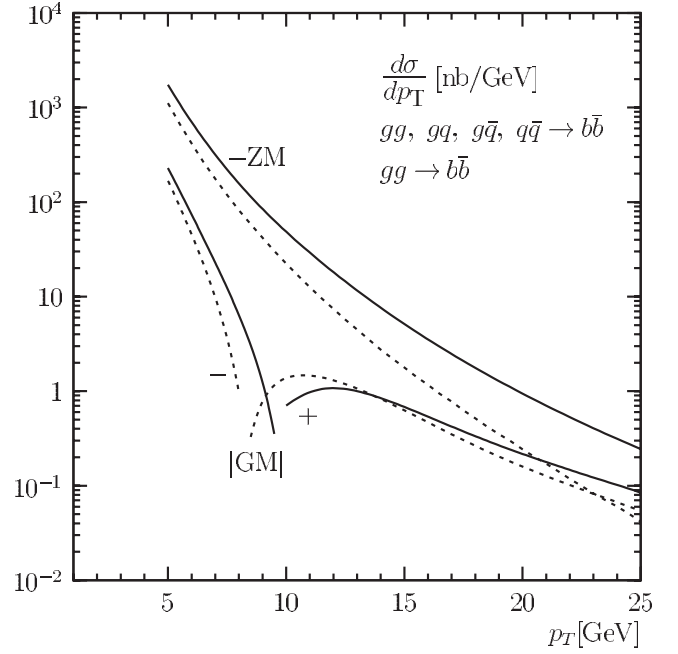


FIG. 4. Transverse-momentum distribution $d\sigma/dp_T$ of $p\bar{p} \rightarrow B + X$ at c.m. energy $\sqrt{S} = 1.96$ TeV integrated over the rapidity range $|y| < 1$. The contributions of class (i) (solid lines) and their gg -initiated parts (dashed lines) evaluated at NLO in the ZM-VFNS (upper lines) and the GM-VFNS (lower lines) are compared.

finite- m effects are washed out in the final predictions, except for very small values of p_T . It is instructive to study the relative importance of the gg -initiated contributions. They are also included in Fig. 4 for $m = 0$ and finite m as the upper and lower dashed lines, respectively. They exhibit a similar pattern as the full class-(i) contributions and dominate the latter in the small- p_T range. Comparing Fig. 4 with Fig. 2(c) in Ref. [14], we observe that the relative influence of the finite- m effects is much smaller in the c -quark case, as expected because the c quark is much lighter than the b quark.

In the remainder of this section, we work in the GM-VFNS and also include the contributions from classes (ii) and (iii), i.e. we allow for b (anti)quarks in the initial state and $g, q, \bar{q} \rightarrow B$ fragmentation. It is interesting to study the relative importance of the various initial states. In Fig. 5, the total result in the GM-VFNS (solid line) is broken up into the contributions from initial states consisting of (1) one gluon and one b (anti)quark (upper dashed line); (2) one q (anti)quark and one b (anti)quark (middle dashed line); (3) two b (anti)quarks (lower dashed line); (4) one gluon and one q (anti)quark or two q (anti)quarks (lower dotted line); and (5) two gluons (upper dotted line). If it were not for the class-(iii) contribution, then the combination of contributions (4) and (5) would coincide with the class-(i) contribution, considered in Fig. 4, and the combination of contributions (1)–(3) would coincide with the

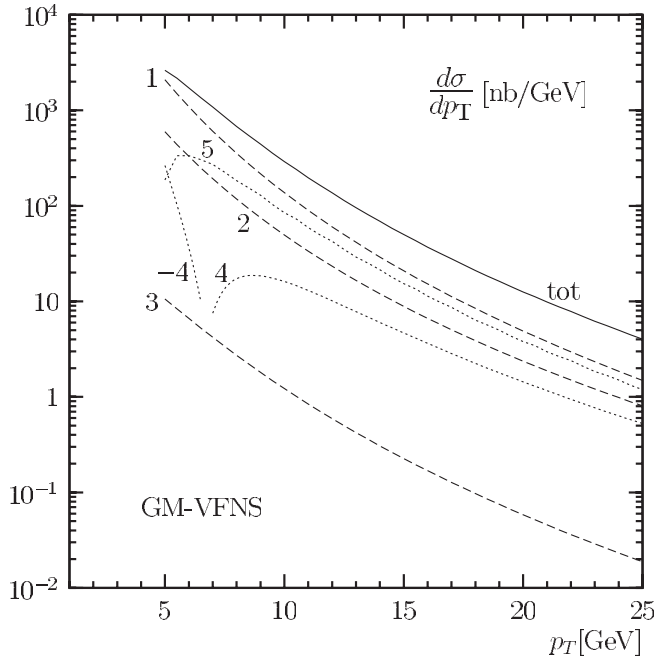


FIG. 5. Transverse-momentum distribution $d\sigma/dp_T$ of $p\bar{p} \rightarrow B + X$ at c.m. energy $\sqrt{s} = 1.96$ TeV integrated over the rapidity range $|y| < 1$. The total NLO result in the GM-VFNS including classes (i)–(iii) (solid line) is broken up into the contributions from initial states consisting of (1) one gluon and one b (anti)quark (upper dashed line); (2) one q (anti)quark and one b (anti)quark (middle dashed line); (3) two b (anti)quarks (lower dashed line); (4) one gluon and one q (anti)quark or two q (anti)quarks; and (5) two gluons.

class-(ii) contribution. However, in Fig. 5, the class-(iii) contribution is distributed among the contributions (1)–(5) according to the respective initial states. We observe from Fig. 5 that the partonic subprocesses with one b or \bar{b} quark in the initial state make up the bulk of the cross section throughout the entire mass range considered. Specifically, the contribution from the subprocesses where the second incoming parton is a gluon (1) is more than twice as large than the one where this is a light (anti)quark (2), and it is even larger than the purely gluon-initiated contribution (5), which is a surprising finding in view of the enormous gluon luminosity in $p\bar{p}$ collisions at a c.m. energy of almost 2 TeV. On the other hand, the contribution from two incoming b (anti)quarks (3) is greatly suppressed, being less than 1% of the full result. The contribution due to light-parton initial states with no more than one gluon (4) ranks between contributions (2) and (3), and it is negative for $p_T \lesssim 7$ TeV. As explained above, the difference between the gg -initiated GM-VFNS contributions in Figs. 4 (lower dashed line) and 5 (upper dotted line) is due to $g, q, \bar{q} \rightarrow B$ fragmentation being included in the latter. Obviously, this additional contribution is quite significant throughout the whole p_T range considered. Comparing the difference between the class-(i) contributions in the ZM-

VFNS and the GM-VFNS in Fig. 4 with the total result in Fig. 5, we anticipate that the finite- m effects on the latter will be rather moderate, except for very small values of p_T , where the ZM-VFNS is expected to break down anyway. Also taking into account that the class-(i) contributions considered in Fig. 4 are less negative (or even positive) in the GM-VFNS than they are in the ZM-VFNS, we conclude that the finite- m effects will moderately enhance the cross section. This point will be subject to further investigation in the next section.

IV. COMPARISON WITH CDF DATA

We are now ready to compare our NLO predictions for the cross section distribution $d\sigma/dp_T$ with Tevatron data. We focus our attention on the more recent CDF data from run II published in Refs. [2,3]. This comparison is presented for the GM-VFNS in Fig. 6, where the solid line represents the central prediction, for $\xi_R = \xi_F = 1$, and the dashed lines indicate the maximum and minimum values obtained by independently varying ξ_R and ξ_F in the range

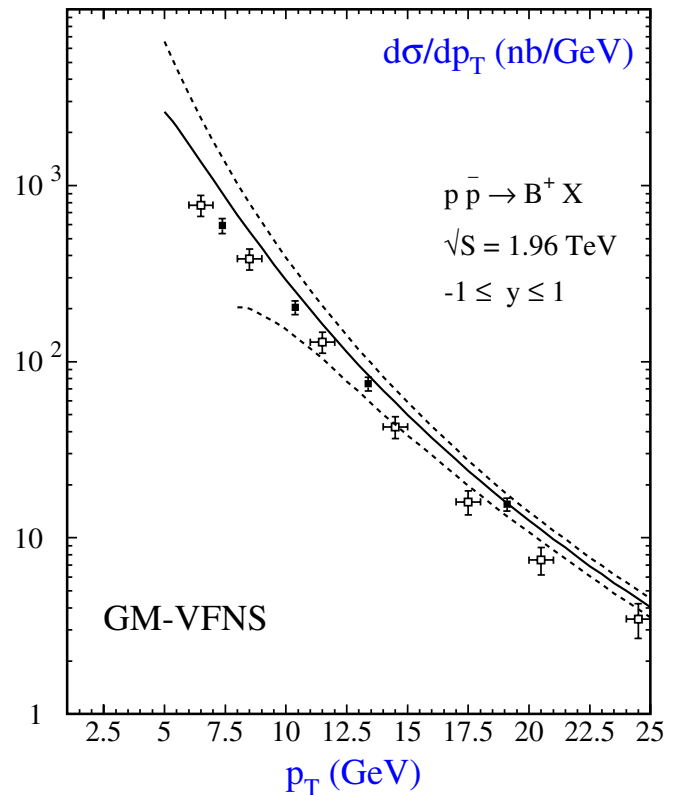


FIG. 6 (color online). Transverse-momentum distribution $d\sigma/dp_T$ of $p\bar{p} \rightarrow B + X$ at c.m. energy $\sqrt{s} = 1.96$ TeV integrated over the rapidity range $|y| < 1$. The central NLO prediction with $\xi_R = \xi_F = 1$ (solid line) of the GM-VFNS is compared with CDF data from Refs. [2] (open squares) and [3] (solid squares). The maximum and minimum values obtained by independently varying ξ_R and ξ_F in the range $1/2 \leq \xi_R, \xi_F \leq 2$ with the constraint that $1/2 \leq \xi_R/\xi_F \leq 2$ are also indicated (dashed lines).

$1/2 \leq \xi_R, \xi_F \leq 2$, with the constraint that $1/2 \leq \xi_R/\xi_F \leq 2$. The maximum and minimum values correspond to $\xi_F = 2$ and $\xi_F = 1/2$, respectively. The variation with ξ_R is considerably milder than the one with ξ_F and only leads to a modest broadening of the error band. For $\xi_F < 1$, μ_F reaches the starting scale $\mu_0 = m$ for the DGLAP evolution of the FFs and the b -quark PDF at $p_T = m\sqrt{1/\xi_F^2 - 1}$. For smaller values of p_T , there is no prediction because the FFs and the b -quark PDF are put to zero for $\mu_F < \mu_0$. This explains why the p_T distribution for $\xi_F = 1/2$ only starts at $p_T = \sqrt{3}m \approx 7.8$ GeV. The most recent data [3] nicely agree with the GM-VFNS result. In fact, they lie close to the central prediction, with a tendency to fall below it in the lower p_T range, and they are comfortably contained within the theoretical error band. Obviously, the notorious Tevatron B -meson anomaly, with data-to-theory ratios of typically 2–3 [1], that has been with us for more than a decade has finally come to its end, thanks to both experimental and theoretical progress (see also Ref. [29] for a recent status report on the observed and predicted cross sections at the Tevatron). The previous CDF data [2], based on a measurement of $J/\psi + X$ final states, are compatible with the latest ones for $p_T \lesssim 12$ GeV, but systematically undershoot them for larger values of p_T . This potential inconsistency becomes even more apparent by noticing that Fig. 6 only contains 4 out of the 13 data points for $p_T > 12$ GeV quoted in Ref. [2] and that the omitted data points neatly line up with the selected ones. This possibly suggests that the systematical errors in Ref. [2], and perhaps also in Ref. [3], might be underestimated and that the overall normalization might need some adjustment. Incidentally, the preliminary CDF data [4] fall right in the middle between those from Refs. [2,3].

The measured p_T distribution of Ref. [2] reaches down to $p_T = 0$ and exhibits a maximum at $p_T \approx 2.5$ GeV. As we shall see below, this small- p_T behavior is correctly reproduced in the FFNS without DGLAP-evolved FFs, which only receives contributions of class (i) without any subtractions. It is clear that our present implementation of the GM-VFNS is not suitable for cross section calculations in the small- p_T region. Although the GM-VFNS is designed to approach the FFNS and the ZM-VFNS in its regions of validity without introducing additional ad-hoc matching factors, to implement this numerically is a non-trivial task due to necessary cancellations between different terms in the calculation. Stable computer codes including these features have been developed for the fully inclusive case and are used in global analyses of proton PDFs, e.g. in the CTEQ studies [25] using the ACOT scheme [18]. For one-particle inclusive processes, the problem to achieve such cancellations is complicated by the extra factorization scale; to obtain a smooth transition from the GM-VFNS to the FFNS, one has to carefully

match terms that are taken into account at fixed order with terms that are resummed to higher orders in the PDFs and FFs. In addition, it remains to be investigated whether a proper scale choice in the small- p_T range is required and helpful to ensure that the FFs and b -quark PDF are sufficiently suppressed already at $p_T = \mathcal{O}(m)$.

The GM-VFNS prediction in Fig. 6 exhibits a sizeable scale uncertainty for $p_T \lesssim 2m$. As mentioned above, the p_T distribution for $\xi_F = 1/2$ only starts at $p_T \approx 7.8$ GeV. These undesirable features will eventually be removed once the matching with the FFNS is specified and implemented. This is a so-called implementation issue [30] that needs to be added on top of the definition of the pure GM-VFNS. This is beyond the scope of the present paper, which is concerned with the intermediate p_T range, and will be treated in a future publication. At this point, we would like to recall how this implementation issue is handled for the FONLL scheme [10]. In that scheme, the FFNS and ZM-VFNS calculations are merged in such a way that the contribution that is added on to the FFNS result, i.e. the ZM-VFNS result with the zero-mass limit of the FFNS result subtracted, is multiplied by a weight function of the form $p_T^2/(p_T^2 + c^2m^2)$ with $c = 5$ to model a smooth transition. Furthermore, the variable p_T of the subtracted ZM-VFNS contribution is shifted to become m_T . In the region where the ZM-VFNS prediction has a large scale uncertainty, i.e. where p_T is 2–3 times larger than m say, this weight function is still rather small, ranging from 14% to 26%. Thus, this weight function not only smoothens the transition, but also ensures that the sizeable theoretical uncertainty of the ZM-VFNS component in the transition region is not reflected in the FONLL prediction, creating the impression that the latter has a small theoretical error. Of course, this source of theoretical uncertainty unavoidably resurfaces when the form of the weight function, which is *a priori* unknown, is varied, e.g. by changing the value of its parameter c . Unfortunately, such a variation is not included in the theoretical error of recent FONLL predictions [11,31].

We now extend our numerical analysis to include the NLO prediction in the FFNS, with $n_f = 4$ massless quark flavors in the initial state, which allows us to also compare with the small- p_T data from Ref. [2]. In the FFNS analysis, we evaluate $\alpha_s^{(n_f)}(\mu_R)$ with $n_f = 4$ and $\Lambda_{\overline{\text{MS}}}^{(4)} = 326$ MeV [25], while we continue using the CTEQ6.1M proton PDFs [25], in want of a rigorous FFNS set with $n_f = 4$. In the FFNS, there is no room for DGLAP-evolved FFs, and only $b, \bar{b} \rightarrow B$ transitions are included. For simplicity, we identify b (anti)quarks with B mesons and account for non-perturbative effects by including the branching fraction $B(b \rightarrow B) = 39.8\%$ [32] as an overall normalization factor, i.e. we use a $b \rightarrow B$ FF of the form $D(x) = B(b \rightarrow B)\delta(1-x)$, while the $g, q, \bar{q} \rightarrow B$ FFs are put to zero. In Fig. 7, the central FFNS (dot-dashed line), ZM-VFNS (dashed line), and GM-VFNS (solid line) predictions, for

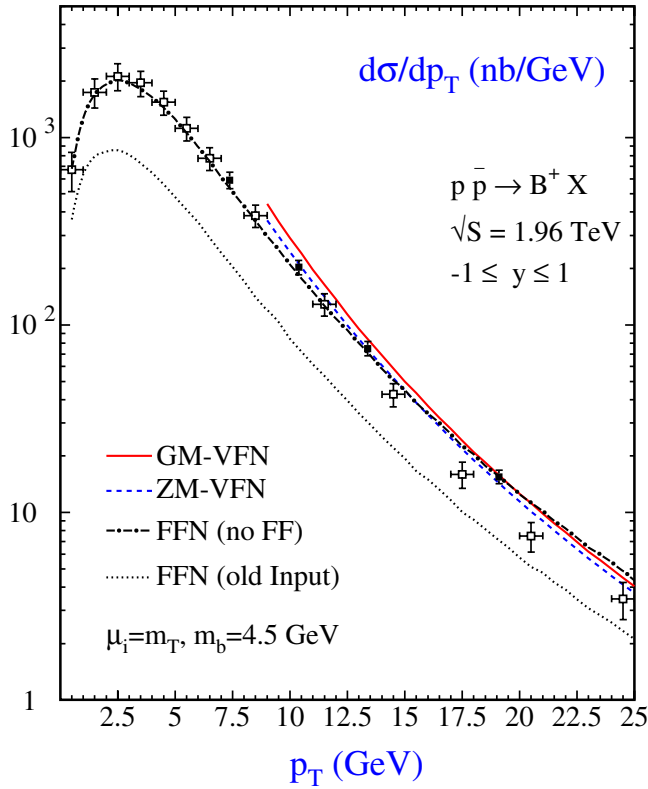


FIG. 7 (color online). Transverse-momentum distribution $d\sigma/dp_T$ of $p\bar{p} \rightarrow B + X$ at c.m. energy $\sqrt{S} = 1.96$ TeV integrated over the rapidity range $|y| < 1$. The central NLO predictions in the FFNS with $n_f = 4$ and without FFs (dot-dashed line), the ZM-VFNS (dashed line), and the GM-VFNS (solid line) are compared with CDF data from Refs. [2] (open squares) and [3] (solid squares). For reference, the historical FFNS prediction, evaluated with PDF set MRSD0 [33], a $b \rightarrow B$ FF of Peterson type [20] with $\epsilon = 0.006$, $m_b = 4.75$ GeV, and $\Lambda_{\overline{\text{MS}}}^{(4)} = 215$ MeV, is also shown.

$\xi_R = \xi_F = 1$, are compared with the CDF data from Refs. [2,3]. As in Fig. 6, some of the data points with $p_T > 7$ GeV from Ref. [2] are omitted for clarity. Since the ZM-VFNS and our present implementation of the GM-VFNS are not applicable to the small- p_T range, we show the respective predictions only for $p_T > 2m = 9$ GeV. The GM-VFNS prediction shown in Fig. 7 is identical with the central one in Fig. 6. By construction, it merges with the ZM-VFNS prediction with increasing value of p_T . In accordance with the expectation expressed in the discussion of Figs. 3 and 4, the difference between the GM-VFNS and ZM-VFNS results is rather modest also at $p_T \gtrsim 2m$, since the m -dependent contribution, of class (i), is numerically small and overwhelmed by the m -independent ones, of classes (ii) and (iii). The FFNS prediction faithfully describes the peak structure exhibited by the next-to-latest CDF data [2] in the small- p_T range and it also nicely agrees with the latest CDF data [3] way out to the largest p_T values. In fact, for $p_T > 4m$, where its

perturbative stability is jeopardized by unresummed logarithms of the form $\ln(m_T^2/m^2) \gtrsim 3$, the FFNS prediction almost coincides with the GM-VFNS one, where such large logarithms are resummed. This is a pure coincidence, which becomes even more apparent if we also recall that the implementation of the $b, \bar{b} \rightarrow B$ transition in the FFNS is not based on a factorization theorem and quite inappropriate for such large values of p_T .

In Figs. 6 and 7, we limited our considerations to the range $p_T < 25$ GeV, where the published CDF data [2,3] are located. However, the preliminary CDF data [4], collected in the very central part of the detector ($|y| < 0.6$), cover the range $9 \text{ GeV} < p_T < 40 \text{ GeV}$, and it is interesting to confront them with the NLO predictions of the three schemes considered here. Moreover, it is instructive to study the breakdown of the FFNS at sufficiently large values of p_T due to unresummed large logarithms. For these purposes, we show in Fig. 8 an extension of Fig. 7 including the preliminary CDF data. We observe that the GM-VFNS result steadily merges with the ZM-VFNS one as the value of p_T is increased, the relative deviations being 11%, 6%, and 3% at $p_T = 20, 30$, and 50 GeV, respectively. The FFNS result breaks even with the GM-VFNS one at about $p_T = 20$ GeV (see also Fig. 7) and exceeds the latter for larger values of p_T , the relative deviations

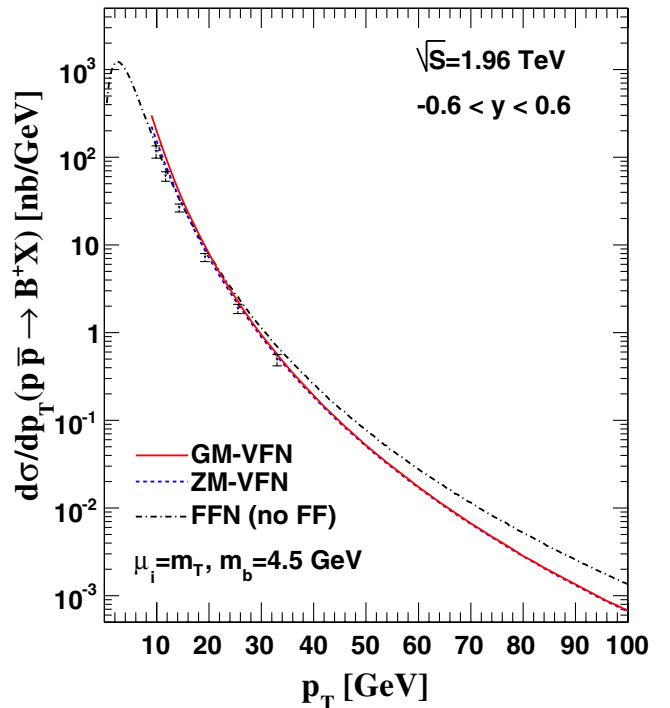


FIG. 8 (color online). Transverse-momentum distribution $d\sigma/dp_T$ of $p\bar{p} \rightarrow B + X$ at c.m. energy $\sqrt{S} = 1.96$ TeV integrated over the rapidity range $|y| < 0.6$. The central NLO predictions in the FFNS with $n_f = 4$ and without FFs (dot-dashed line), the ZM-VFNS (dashed line), and the GM-VFNS (solid line) are compared in the large- p_T range.

being 20%, 48%, and 100% at $p_T = 30, 50,$ and 100 GeV, respectively. Our results indicate that a measurement of the p_T distribution up to 40–50 GeV at the Tevatron could be able to resolve the difference between the FFNS and the VFNS and so to establish for the first time the breakdown of the FFNS due to unresummed logarithms in the inclusive hadroproduction of heavy hadrons. This important question deserves a careful examination of the theoretical uncertainties, which we leave for a future publication. The preliminary CDF data point in the bin $29 \text{ GeV} < p_T < 40 \text{ GeV}$ favors the ZM-VFNS and GM-VFNS results, while it undershoots the FFNS result.

We conclude this section with an interesting observation that, in retrospect, sheds some new light on the Tevatron B -hadron anomaly mentioned above and does not appear to be sufficiently well known to the community. In fact, the common perception that the CDF data [1–3] generally overshoot the FFNS prediction, frequently denoted as NLO QCD in the literature, by a factor of 2–3 is entirely due the use of obsolete theoretical input. In fact, the FFNS prediction that has been serving as a benchmark for some 15 years and still does even in very recent papers [3,29] is evaluated with the proton PDF set MRSD0 by Martin, Roberts, and Stirling [33], which has been revoked by these authors. It has an unacceptably weak gluon and a small value of $\Lambda_{\overline{\text{MS}}}^{(4)}$, namely $\Lambda_{\overline{\text{MS}}}^{(4)} = 215 \text{ MeV}$ translating into $\alpha_s^{(5)}(m_z) = 0.111$, which is 3.3 standard deviations below the present world average $\alpha_s^{(5)}(m_z) = 0.1176 \pm 0.0020$ [32]. Other inputs include $m_b = 4.75 \text{ GeV}$ and a Peterson FF parameter of $\epsilon = 0.006$, extracted from a fit to e^+e^- annihilation data from the pre-LEP/SLC era using a Monte-Carlo event generator based on massless LO matrix elements [34]. For reference, the historical FFNS prediction evaluated with this choice of input is also included in Fig. 7. Since the FONLL prediction [11] is designed to merge with the FFNS one at low values of p_T , the additional contribution being faded out by a weight function of the form $p_T^2/(p_T^2 + 25m_b^2)$, the striking gap between the historical NLO QCD prediction and the FONLL prediction, based on up-to-date input information, in Fig. 10 of Ref. [3] impressively illustrates the advancement in the PDF and α_s determinations. The tuning of FFs in connection with the resummation of leading and next-to-leading logarithms, emphasized in the second paper of Ref. [4], is actually of minor importance.

V. CONCLUSIONS

For several years, the B -meson production rates measured at DESY HERA, CERN LEP2, and Tevatron have been notoriously exceeding, by up to a factor of 3, the usual NLO QCD predictions for massive b quarks, i.e. those in the FFNS (B -meson anomaly). This has even triggered theoretical attempts to interpret this deviation as a signal of new physics beyond the standard model [35]. However,

it remained to be clarified if this deviation could be explained by improving and refining the QCD prediction itself. In this connection, two of us, together with Binnewies, pointed out almost a decade ago that the ZM-VFNS provides a rigorous theoretical framework for a coherent study of B -meson production in high-energy e^+e^- , $p\bar{p}$, and other collisions, since the factorization theorem guarantees the universality of the B -meson FFs [5]. In fact, the ZM-VFNS prediction [5,6] was found to nicely agree with the CDF data from Tevatron runs IA and I [1]. However, a necessary condition for the applicability of the ZM-VFNS is that the energy scale that separates perturbative hard scattering from nonperturbative fragmentation (final-state factorization scale μ_F) is sufficiently large compared to the b -quark mass m , and it had never been quite clear how large the ratio μ_F/m actually needed to be in order for finite- m effects to be negligible. In fact, the authors of Ref. [31] asserted in a footnote that mass corrections have a large size up to $p_T \approx 20 \text{ GeV}$ and that “lack of mass effects [5] will therefore erroneously overestimate the production rate at small p_T .”

In the present paper, we addressed this problem by performing a comparative analysis of B -meson hadroproduction in the ZM-VFNS and the GM-VFNS, which we had successfully applied to D -meson production in $\gamma\gamma$ [12], ep [13], and $p\bar{p}$ [14–16] collisions in the past. For this, we also updated the determination of B -meson FFs [5] by fitting to recent e^+e^- data from ALEPH [22], OPAL [23], and SLD [24] and also adjusting the values of m and the energy scale μ_0 where the DGLAP evolution starts to conform with modern PDF sets [25]. We found that finite- m effects moderately enhance the p_T distribution; the enhancement amounts to about 20% at $p_T = 2m$ and rapidly decreases with increasing value of p_T , falling below 10% at $p_T = 4m$. This finding contradicts earlier claims [31] in all respects. Such effects are comparable in size to the theoretical uncertainty due to the freedom of choice in the setting of the renormalization and factorization scales. For comparison, we also evaluated the p_T distribution in the FFNS, with $n_f = 4$, using a delta-function-type $b \rightarrow B$ FF without DGLAP evolution.

Confronting the three NLO predictions with the latest [3] and next-to-latest [2] CDF data sets published, we found that all of them agree rather well with the latest one, with $p_T > 7 \text{ GeV}$. Despite unresummed large logarithms and poorly implemented fragmentation, the FFNS prediction happens to almost coincide with the GM-VFNS one in the range $15 \text{ GeV} \leq p_T \leq 25 \text{ GeV}$. The FFNS prediction also nicely reproduces the peak exhibited about $p_T \approx 2.5 \text{ GeV}$ by the next-to-latest CDF data [2]. By contrast, the historical benchmark result based on obsolete proton PDFs and a value of $\alpha_s^{(5)}(m_z)$ falling short of the present world average by 3.3 standard deviations, which goes under the name NLO QCD in the literature and is used as a reference point even in most recent papers [3,29],

undershoots the CDF data by the familiar factor of 2–3. This illustrates that the progress in our understanding of the proton PDFs and our knowledge of $\alpha_s^{(5)}(m_Z)$ is instrumental in overcoming the long-standing Tevatron B -hadron anomaly in the low to intermediate p_T range. The preliminary CDF data [4] favor the ZM-VFNS and GM-VFNS results in the upmost bin, $29 \text{ GeV} < p_T < 40 \text{ GeV}$, while they undershoot the FFNS result.

It is desirable to extend the applicability of the GM-VFNS down to $p_T = 0$. This requires matching with the

FFNS. To achieve this in a way that avoids ad-hoc weight functions is a nontrivial task and is left for future work.

ACKNOWLEDGMENTS

The work of B. A. K. and G. K. was supported in part by the German Federal Ministry for Education and Research BMBF through Grant No. 05 HT6GUA and by the German Research Foundation DFG through Grant No. KN 365/7–1.

-
- [1] F. Abe *et al.* (CDF Collaboration), *Phys. Rev. Lett.* **75**, 1451 (1995); D. Acosta *et al.* (CDF Collaboration), *Phys. Rev. D* **65**, 052005 (2002).
- [2] D. Acosta *et al.* (CDF Collaboration), *Phys. Rev. D* **71**, 032001 (2005).
- [3] A. Abulencia *et al.* (CDF Collaboration), *Phys. Rev. D* **75**, 012010 (2007).
- [4] J. A. Kraus, Ph.D. thesis, University of Illinois [Institution Report No. FERMILAB-THESIS-2006-47, 2006 (unpublished)]; A. Annovi (on behalf of the CDF Collaboration), FERMILAB Report No. FERMILAB-CONF-07-509-E, 2007 (to be published).
- [5] J. Binnewies, B. A. Kniehl, and G. Kramer, *Phys. Rev. D* **58**, 034016 (1998).
- [6] B. A. Kniehl and G. Kramer, *Phys. Rev. D* **60**, 014006 (1999); B. A. Kniehl, in *Proceedings of the 14th Topical Conference on Hadron Collider Physics (Hadron Collider Physics 2002)*, 2002, edited by M. Erdmann and Th. Müller (Springer, Berlin, 2003), p. 161.
- [7] M. Cacciari and M. Greco, *Nucl. Phys.* **B421**, 530 (1994).
- [8] It is, therefore, misleading to refer to NLO calculations in the ZM-VFNS as NLL calculations, as is sometimes done.
- [9] P. Nason, S. Dawson, and R. K. Ellis, *Nucl. Phys.* **B303**, 607 (1988); **B327**, 49 (1989); **B335**, 260(E) (1990); W. Beenakker, H. Kuijff, W. L. van Neerven, and J. Smith, *Phys. Rev. D* **40**, 54 (1989); W. Beenakker, W. L. van Neerven, R. Meng, G. A. Schuler, and J. Smith, *Nucl. Phys.* **B351**, 507 (1991); I. Bojak and M. Stratmann, *Phys. Rev. D* **67**, 034010 (2003).
- [10] M. Cacciari, M. Greco, and P. Nason, *J. High Energy Phys.* 05 (1998) 007.
- [11] M. Cacciari and P. Nason, *Phys. Rev. Lett.* **89**, 122003 (2002).
- [12] G. Kramer and H. Spiesberger, *Eur. Phys. J. C* **22**, 289 (2001); **28**, 495 (2003).
- [13] G. Kramer and H. Spiesberger, *Eur. Phys. J. C* **38**, 309 (2004).
- [14] B. A. Kniehl, G. Kramer, I. Schienbein, and H. Spiesberger, *Phys. Rev. D* **71**, 014018 (2005).
- [15] B. A. Kniehl, G. Kramer, I. Schienbein, and H. Spiesberger, *Eur. Phys. J. C* **41**, 199 (2005).
- [16] B. A. Kniehl, G. Kramer, I. Schienbein, and H. Spiesberger, *Phys. Rev. Lett.* **96**, 012001 (2006).
- [17] G. Alexander *et al.* (OPAL Collaboration), *Phys. Lett. B* **364**, 93 (1995).
- [18] M. A. G. Aivazis, J. C. Collins, F. I. Olness, and W.-K. Tung, *Phys. Rev. D* **50**, 3102 (1994).
- [19] F. I. Olness, R. J. Scalise, and W.-K. Tung, *Phys. Rev. D* **59**, 014506 (1998).
- [20] C. Peterson, D. Schlatter, I. Schmitt, and P. M. Zerwas, *Phys. Rev. D* **27**, 105 (1983).
- [21] V. G. Kartvelishvili and A. K. Likhoded, *Yad. Fiz.* **42**, 1306 (1985) [*Sov. J. Nucl. Phys.* **42**, 823 (1985)].
- [22] A. Heister *et al.* (ALEPH Collaboration), *Phys. Lett. B* **512**, 30 (2001).
- [23] G. Abbiendi *et al.* (OPAL Collaboration), *Eur. Phys. J. C* **29**, 463 (2003).
- [24] K. Abe *et al.* (SLD Collaboration), *Phys. Rev. Lett.* **84**, 4300 (2000); *Phys. Rev. D* **65**, 092006 (2002); **66**, 079905(E) (2002).
- [25] J. Pumplin, D. R. Stump, J. Huston, H.-L. Lai, P. Nadolsky, and W.-K. Tung (CTEQ Collaboration), *J. High Energy Phys.* 07 (2002) 012; D. Stump, J. Huston, J. Pumplin, W.-K. Tung, H.-L. Lai, S. Kuhlmann, and J. F. Owens (CTEQ Collaboration), *ibid.* 10 (2003) 046.
- [26] B. A. Kniehl and G. Kramer, *Phys. Rev. D* **74**, 037502 (2006).
- [27] J. Binnewies, B. A. Kniehl, and G. Kramer, *Phys. Rev. D* **58**, 014014 (1998); B. A. Kniehl and G. Kramer, *ibid.* **71**, 094013 (2005).
- [28] F. Aversa, P. Chiappetta, M. Greco, and J. Ph. Guillet, *Phys. Lett. B* **210**, 225 (1988); **211**, 465 (1988); *Nucl. Phys.* **B327**, 105 (1989).
- [29] F. Happacher, P. Giromini, and F. Ptohos, *Phys. Rev. D* **73**, 014026 (2006).
- [30] W. K. Tung, S. Kretzer, and C. Schmidt, *J. Phys. G* **28**, 983 (2002).
- [31] M. Cacciari, S. Frixione, M. L. Mangano, P. Nason, and G. Ridolfi, *J. High Energy Phys.* 07 (2004) 033.
- [32] W. M. Yao *et al.* (Particle Data Group), *J. Phys. G* **33**, 1 (2006).
- [33] A. D. Martin, W. J. Stirling, and R. G. Roberts, *Phys. Rev. D* **47**, 867 (1993).
- [34] J. Chrin, *Z. Phys. C* **36**, 163 (1987).
- [35] E. L. Berger, B. W. Harris, D. E. Kaplan, Z. Sullivan, T. M. P. Tait, and C. E. M. Wagner, *Phys. Rev. Lett.* **86**, 4231 (2001).